Rheological Investigation on the Interaction of Polyamide 6 with Clay

Tong Wan,[1] Biao Wang,[1] Shuang Liao,[1] Mike Clifford[2]

[1]*College of Material Science and Chemical Engineering, Tianjin University of Science and Technology, Tianjin 300457, People's Republic of China*
[2]*School of Mechanical, Materials, Manufacturing Engineering and Management Faculty of Engineering, The University of Nottingham, University Park, Nottingham NG7 2RD, United Kingdom*

Received 4 July 2011; accepted 29 August 2011
DOI 10.1002/app.35554
Published online 19 December 2011 in Wiley Online Library (wileyonlinelibrary.com).

ABSTRACT: The interaction of polyamide 6 (PA) with clay is studied via rheological approaches. The relationship of the effective viscosity (η_r), the clay volume fraction (Φ_{clay}), the aspect ratio (P), and the critical volume fraction (Φ_c) is built up by using the Maron-Pierce model. The time–temperature superposition (TTS) is applied to evaluate the relaxation of PA in the presence of clay under various temperatures. Furthermore, the modified Cox-Merz rule is used to build up the viscosity response of PA/clay nanocomposites under both dynamic shear and steady shear. © 2011 Wiley Periodicals, Inc. J Appl Polym Sci 125: E27–E33, 2012

Key words: clay; rheology; Maron-Pierce model

INTRODUCTION

Polyamide/clay nanocomposites (PA/clay) represent an attempt to improve many properties due to a high exfoliation of clay and good interfacial compatibility between clay layers and PA matrix. Clay as a nanoscale reinforcement contributes to an increase in the mechanical properties of the conventional fiber composites.[1] Much interest has been focused on the rheological properties of nanocomposites, based on various polymer systems.[2–6]. PA/clay exhibit pseudo solid-like behavior and yield stress in response to a small dynamic shear.[7,8] Higher viscosity and shear thinning can be observed with the addition of clay at a relatively low shear rate, at which the matrix exhibits a Newtonian response.[9] The results can be attributed to high exfoliation, high aspect ratio of clay, and strong interaction between clay and PA. The ionized amide groups provide positive charges to neutralized negative charges on the clay surface, so the ionic interaction may exist between PA and clay. In addition, the tremendous specific area surfaces of clay may absorb and entangle PA chains in the nanoscale. Currently, how the interaction affects the rheology of nanocomposites in molten state is not readily understood. Theoretical studies have been carried out on the rheology of micronscale filler filled polymers with various shapes, such as spheres, rods, discs, and fibers.[10] The Maron-Pierce model is valid for micronscale filler filled polymers.[11] However, dispersion of clay in matrix is complicated by the presence of interaction between polymers and clay. Few models describe the effective viscosity (η_r) dependence of clay filled nanocomposites. This article attempts to use the Maron-Pierce model to study and build up the relationship of four variables η_r, Φ_{clay}, P, and Φ_c, and further explore the interaction of PA and clay.

The interesting fact is whether the interaction of clay with PA affects validity of time-temperature superposition (TTS) or not in the linear viscoelastic range. TTS is widely used to make a master curve and extend the frequency regime at a given temperature.[12] In most cases, TTS is valid for suspensions without interaction because the relaxation process of melts corresponds to the same temperature dependence. In some cases, TTS is not hold for suspensions with strong interaction because more than one relaxation mechanism takes place which correspond to the different temperature dependence. Thus, the interaction in nanoscale of melts can be evaluated by validity of TTS. In this article, van-Gurp-Palmen plot is applied under dynamic shear with various temperatures to determine the validity of TTS.

Correspondence to: T. Wan (wantong@tust.edu.cn).
Contract grant sponsor: The University of Nottingham, UK, for issuing University Research Scholarship (URS).
Contract grant sponsor: Scientific Research Foundation of Tianjin University of Science & Technology; contract grant number: 0000401.
Contract grant sponsor: Scientific Research Foundation for the Returned Overseas Chinese Scholars (SRF for ROCS); contract grant number: 0000201.
Contract grant sponsor: State Education Ministry (SEM).

The Cox-Merz rule is applied to characterize the response of PA/clay nanocomposites under dynamic and steady shear. The Cox-Merz rule is an empirical relationship to build up the viscosity relationship between dynamic and steady shear conditions. For virgin polymers, steady viscosity (η) and dynamic viscosity (η^*) are superposed at the same values of angular frequency (ω) and steady shear rate ($\dot{\gamma}$): $\eta^*(\omega) = \eta(\dot{\gamma})|_{\omega=\dot{\gamma}}$. However, some of the complex melts associated with strong interactions at the molecular level are deviated from the Cox-Merz rule.[13–16] In this article, another important feature is to predict the influences of clay on the deviation of the Cox-Merz rule under steady and dynamic shear. We expect that the rheological studies gain herewith could give more knowledge in understanding the interaction of nano-fillers and polymeric matrix in nanocomposites.

EXPERIMENTAL

Materials

Ultramid B3 Polyamide 6 (PA) is a commercial product supplied by BASF. Clay is Cloisite 30B supplied by Southern Clay Company, which is a white powder containing montmorillonite (70 wt %) intercalated with an organo modifier (30 wt %), d_{001} = 1.85 nm. All materials are dried at 80°C under vacuum before rheological tests.

Preparation of PA/clay nanocomposites

PA and clay are co-fed into a twin screw extruder with screw aspect ratio L/D = 24 : 1 at 240°C. The screw speed is set at 400 rpm to provide sufficient shear in the melt compounding process. The extruded strands are palletized and dried under vacuum at 80°C for 10 h before testing. Nanocomposites with various clay loading is denoted as PA/clay − *n*, where *n* (*n* = 1, 3, 5, 8, 10) is the mass fraction of clay. Sample disks for rheology measurements are prepared by compressing the extruded pellets at 240°C for 3 min.

Density measurements of PA/clay nanocomposites

The AccuPyc 1330 Pycnometer is used to measure the density of samples. It determines volume by measuring the pressure change of helium in a calibrated volume. Samples are weighted on a digital scale (accuracy 0.1 mg). The analyzer measures the volume of the samples, from which density can be derived. Five tests are used for each sample.

Rheology measurements of PA/clay nanocomposites

Rheology measurements are conducted on a Bohlin CVOR200 Rheometer. For steady viscosity measurements, the tests are performed under steady shear and loaded into a pair of cone-plates with 25 mm diameter and 0.5 mm gap size. For effective viscosity studies, the applied shear stress ranges from 100 to 2000 Pa at 240°C to eliminate the yield stress contribution to the viscosity. For TTS studies, all tests are performed via dynamic viscosity measurements and loaded into a pair of parallel plates with 25 mm diameter and 1 mm gap size. The angular frequency sweep ranges from 0.1 to 100 rad/s at low strain amplitude to ensure that the measurements are taken well within the linear viscoelastic range. All tests are conducted from 230 to 270°C at 10°C interval. For Cox-Merz rule studies, the viscosity responses under dynamic and steady shear are loaded into a pair of parallel plates with 25 mm diameter and 1mm gap size. The applied steady shear rate ranges from 0.01 to 10 s^{-1} to ensure no slippage. The applied angular frequency sweep ranges from 0.1 to 10 rad/s. All measurements are conducted under a nitrogen atmosphere to avoid oxidative degradation of the specimens.

RESULTS AND DISCUSSION

Theory for prediction of effective viscosity

For the filler suspension, an effective viscosity (η_r) can be defined as the ratio of the viscosity of the suspension (η_Φ) to that of the matrix (η_o) at the same shear stress, and it is assumed to be a function of the filler volume fraction Φ.

$$\eta_r = \eta_\Phi / \eta_o \tag{1}$$

The most common equation based on the Einstein equation is that η_r is a function of Φ the suspension by a power series expansion with high order terms.[17]

$$\eta_r = 1 + k_1\Phi + k_2\Phi^2 + k_3\Phi^3 + \ldots\ldots \tag{2}$$

To take account of the filler-shape in the suspensions, it is not universally acknowledged and more complex.[18,19] Apart from the ideal case of fillers, anisometric fillers have at least one distinguished direction along in which their size is significantly larger. The simplest way to qualify shapes for real anisometric fillers is by their aspect ratio. Aspect ratio (*P*) is defined as the ratio of the largest to the smallest dimension of a filler. For real filler systems, which are usually polydisperse with respect to size and shape, the determination of the aspect ratio is not an easy task. In reality an average aspect ratio can be calculated for the system as a whole.

There have been numerous attempts to find expressions that extend the validity of the power law. η_r of filled melts can be assumed to be a function of the filler volume fraction Φ and the critical

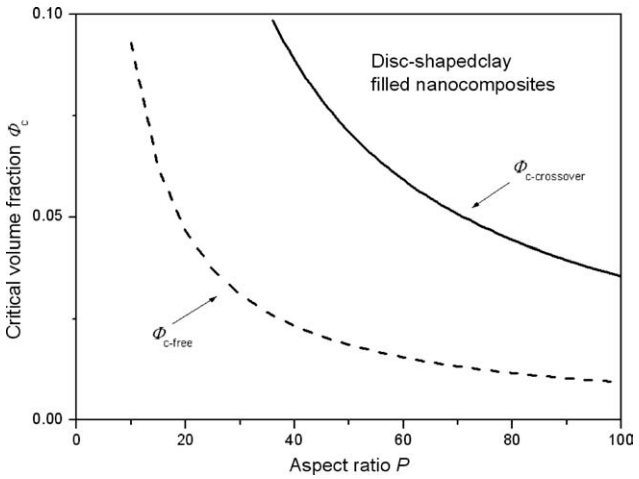

Figure 1 Critical free rotation volume fraction $\Phi_{c\text{-free}}$ and crossover volume fraction $\Phi_{c\text{-crossover}}$ versus average aspect ratio P.

volume fraction Φ_c as the Maron-Pierce model stated.

$$\eta_r = \left(1 - \frac{\Phi}{\Phi_c}\right)^{-2} \tag{3}$$

The Maron-Pierce model is an empirical equation which can be used for non-Newtonian suspensions. It is widely used and recommended for the various composites filled with inorganic fillers, glassy spheres, and fibers.[20–22] The effect of η_r has been studied, including the average aspect ratio, volume fraction, and distribution of fiber length. The studies find that the equation has a simple form, and is considered to have a practical utility for filled composites when the shear stress is larger than yield stress to eliminate the yield stress contribution to viscosity.

For disc-shaped filler suspensions,[23] the critical free rotation volume fraction $\Phi_{c\text{-free}}$ is a function of P and can be written as

$$\Phi_{c\text{-free}} = 0.93/p \tag{4}$$

If the concentration of fillers exceeds the limit of possible free rotation ($\Phi_{clay} > \Phi_{c\text{-free}}$), then the filler-to-filler interactions become stronger and the circular discs cannot rotate freely. A distribution of clay from disordered to ordered state spontaneously occurs at very low Φ and P. The crossover volume fraction ($\Phi_{c\text{-crossover}}$) is a function of P at the equal amounts of the ordered and disordered states.[24] The relationship between $\Phi_{c\text{-crossover}}$ and P can be approximated as

$$\Phi_{c\text{-crossover}} = 3.55/p \tag{5}$$

Figure 1 shows that the critical volume fraction $\Phi_{c\text{-free}}$ and $\Phi_{c\text{-crossover}}$ of clay as a function of P predicted by eqs. (4) and (5). $\Phi_{c\text{-free}}$ and $\Phi_{c\text{-crossover}}$ for disc-shaped clay decrease with the increase of P and a lower $\Phi_{c\text{-crossover}}$ can be observed for clay compared to $\Phi_{c\text{-free}}$. According to Figure 1, it is essential to estimate P so that the distribution of clay in the matrix can be determined.

Since the thickness of an individual disk-like clay platelet is 1 nm, the diameter of clay and the extent of exfoliation is related to P.[25] Previous studies show the average aspect ratio P varies from 87 to 132 for clay prepared by the in situ polymerization,[26] whereas it is 57 for clay prepared by the melt compounding process.[27] According to wide-angle X-ray analysis, Cloisite 30B has a repeat spacing of 1.85 nm, in which the thickness of an organic modifier is about 0.90 nm. In this study, the predicted range of P for PA/clay is determined by adjusting the η_r and Φ_c according to Maron-Pierce model.

Modeling of effective viscosity of PA/clay nanocomposites

Density analysis is needed to predict density and volume fraction, since the Maron-Pierce model for viscosity prediction is based on the volume fraction of fillers rather than mass fraction. The densities can be used to calculate the volume fraction of fillers. The density of PA is 1.14 g/cm^3, which is exactly the same as the density provided by the supplier. Previous studies showed that Cloisite 30B contains 30 wt % of modifiers.[28] Φ_{clay} of Cloisite 30B is predicted after deducting the volume of modifiers. It is difficult to find the density of the modifier from references, but the densities of organic-clay is 1.61 g/cm^3.[29] The density of the modifier can be calculated as 0.8 g/cm^3. It is similar to the density of octadecane (0.777 g/cm^3) which has a similar chemical structure to the modifier. The volume fraction of clay can be written as eq. (6). According to eq. (6) and experimental data, Φ_{clay} is calculated. Thus, it is expected that the Φ_{clay} calculated from eq. (6) is reasonable and can be used for the Maron-Pierce model.

$$\Phi_{clay} = \frac{m_{clay}/\rho_{clay}}{m/\rho} \tag{6}$$

in which Φ_{clay} is the volume fraction of clay; ρ, ρ_{clay}, and ρ_m are the densities of the nanocomposite, clay, and matrix, respectively; m and m_{clay} are the mass of the nanocomposite and clay respectively.

The densities of samples, PA/clay-n, where n (n = 1, 3, 5, 8, 10), is determined by the AccuPyc 1330 Pycnometer. The Φ_{clay} calculated from eq. (6) for PA/clay-3, 5, 8, 10 are 0.009, 0.0143, 0.023, and 0.029, respectively.

Figure 2 shows η_r versus shear stress (τ) of PA/clay. Non-Newtonian behavior flows can be

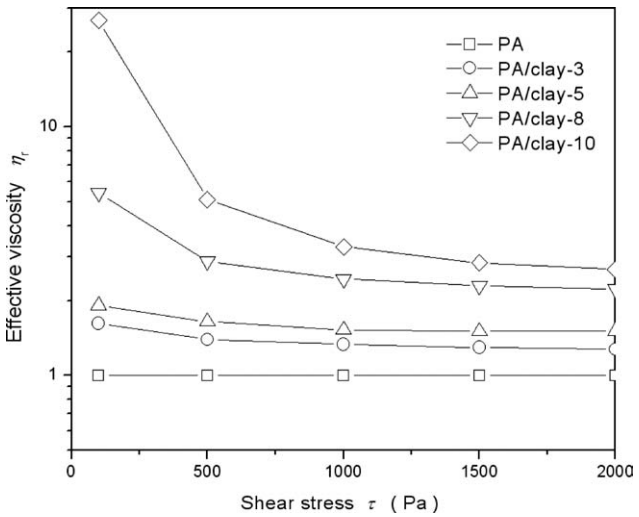

Figure 2 Effective viscosity η_r as a function of shear stress τ of PA/clay nanocomposites.

observed for PA/clay with increasing clay loading. PA/clay exhibit Non-Newtonian behavior after τ_y, so the Herschel-Bulkley model is applied for estimating the yield stress. The yield stress of PA/clay-3, 5, 8, 10 are 0, 2, 7, 18 Pa, respectively. The shear stress is applied over 100 Pa to eliminate the yield stress contribution to viscosity. The Maron-Pierce model has been used in recent research on the filler filled composites.[22,23] It is considered to have a practical utility for filled composites when the shear stress ranges far more over the yield stress. η_r of PA/clay versus τ in the ranges from 1×10^2 Pa to 2×10^3 Pa at 240°C is calculated and plotted in Figure 2. The slope of the curve reflects the change of viscosity since η_r of PA is normalized to 1. For all of PA/clay, an increase of η_r can be observed with increasing clay loading. Furthermore, the influence of clay loading on η_r is predominant at low τ rather than at high τ.

As shown in Figure 3, η_r of PA/clay is predicted from the Maron-Pierce model according to Kataoka approaches. When P equals 50, the model can be fitted according to the prediction from eq. (5) rather than eq. (4). The results demonstrate that the distribution of clay in the matrix is the combination of ordered and disordered state during the shear stress ranged from 1×10^2 Pa to 2×10^3 Pa. $\eta_r^{-1/2}$ diverges from the predicted curve at the low τ. The most probable reason for the disparity is that nanoscale clay has a very large specific area surface in the order of 50 to 800 m^2/g with occupied negative charges. Dispersion of clay in PA melts is complicated by the presence of electrostatic forces, which results in strong interaction and entanglement between amide groups of PA with clay. The actual viscosity of nanocomposites at low τ is much higher than the prediction, so the high interaction between clay and PA can not be neglected at the low τ. It is plausible that if the entanglement layer of polymer on the clay surface is assumed as a part of volume fraction of clay, the effective volume fraction is higher than the actual volume fraction of clay. Thus, the Maron-Pierce model may be applicable for the predictions. The relationship between clay loading and η_r can be built up according to eq. (7).

$$\eta_r^{-1/2} = 1 - \frac{k\Phi_{\text{clay}}}{\Phi_c} \tag{7}$$

An effective volume fraction can be restated as $k\Phi_{\text{clay}}$ k is set as entanglement ability parameter to add in the Maron-Pierce model. The expected linearity between $\eta_r^{-1/2}$ and Φ_{clay} is confirmed, allowing for an explicit determination of k for PA/clay. The prediction values of k for PA/clay at various shear stresses 100, 500, 1000, 1500, and 2000 Pa are 1.93, 1.34, 1.10, 1.01, and 0.98 respectively.

From this study, the effect of clay on the η_r can be predicted by the Maron-Pierce model, taking into account the entanglement of PA on the clay surface. Using the approximation of eq. (7), the entanglement layer can be predicted from the Maron-Pierce model. The entanglement layer has a significant effect on the clay surface. Evidently, as the P of PA/clay is 50, strong interaction and entanglement on the clay surfaces decreases with increasing shear stress. Even though this prediction is a relative value, the Maron-Pierce model can be used to explain the significantly high viscosity of PA/clay beyond the yield stress. This interaction on the clay surface causes different chain relaxation and alters the temperature response of PA/clay.

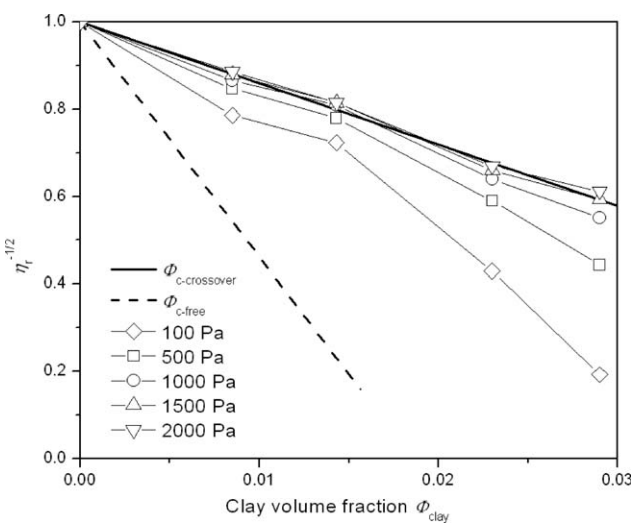

Figure 3 $\eta_r^{-1/2}$ as a function of the ratio of clay volume fraction Φ_{clay} (open symbols are the experiment data, the black line using $\Phi_{\text{c-crossover}}$, and the red line using $\Phi_{\text{c-free}}$ predicted by the Maron-Pierce model).

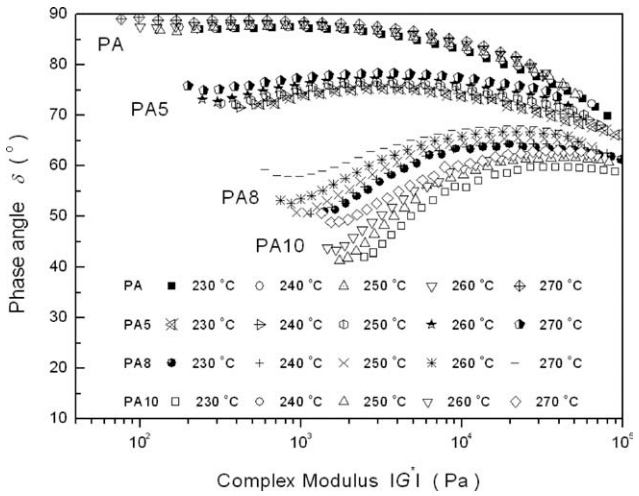

Figure 4 Time–temperature superposed phase angle as a function of complex modulus for PA/clay-*n* at a reference temperature of 240°C.

Time–temperature superposition (TTS) for PA/clay nanocomposites

In order to evaluate the effect of temperature on the microstructure of PA/clay nanocomposites, TTS has been studied by van-Gurp-Palmen plot as an indicator. This plotting method eliminates the effect of vertical shifting along the modulus axis. If TTS holds, phase angle (δ) ($\delta = \text{atan}(G''/G')$, in which G'' is viscous modulus; G' is elastic modulus) is independent of temperature and yields a master curve. δ versus the complex modulus ($|G^*|$) is plotted in Figure 4. The curves of PA show that a master curve can be created and yields temperature independent curve. With clay loading increasing, the failure of TTS is more prominent for PA/clay nanocomposites. Generally the conventional fillers do not influence the relaxation mechanism of PA, and in practice no influence of fillers and PA molecular weight on the activation energy is found. However, additions of clay cause a clear failure of TTS at the low frequencies. The extent of failure of TTS increases with clay loading. For example, PA/clay-10 needs a considerable vertical shift in the superposition procedure. In principle, failure of TTS could be observed because the physical microstructure of the material changes with temperature. A well-known example is long chain branched polymers such as LDPE which does not obey TTS, because the branched chains will influence the relaxation mechanism.[30] The failure of TTS could be subtle observed for PA/clay because the relaxation of PA on clay surface is different from that of matrix.

Cox-Merz rule for PA/clay nanocomposites

The Cox-Merz rule is applied in order to study the viscosity relationship between dynamic and steady shear conditions. It has been confirmed for most virgin polymers that η (steady viscosity) and η* (dynamic viscosity) are superposed at the same values of angular frequency (ω) and steady shear rate ($\dot{\gamma}$). However, some of the complex polymer blends do not follow the Cox-Merz rule. Previous studies show that the deviations from the Cox-Merz rule for complex melts are associated with strong interactions and complex structures at the molecular level for gels and crosslinked systems.[31] It is a valuable approach for studying the microstructure of nanocomposites and the influence of clay on nanocomposites under the two types of shears, since structural and interaction information can be implied. In Figure 5, the Cox-Merz rule is used to characterize the response of PA/clay under large deformation (steady shear) and small deformation (dynamic shear). η* and η are plotted against ω and $\dot{\gamma}$. $\dot{\gamma}$ ranges from 0.1 to 10 s^{-1} to eliminate the yield stress effect on steady viscosity. η* and η of PA vary between 250 and 180 Pa·s and do not exhibit significant shear thinning, so they can be overlaid and exhibit Newtonian behavior. The Cox-Merz rule $\eta^* = \eta|_{\omega=\dot{\gamma}}$ fits well for all ω and $\dot{\gamma}$ measured ranges for PA. PA/clay exhibit shear thinning behavior, which is more pronounced with an increase of clay loading. The deviation of the Cox-Merz rule can be observed for PA/clay and increases with clay loading. When $\dot{\gamma}$ and ω are equal, η* is noticeably larger than η for PA/clay. It should be noted that η is slightly lower than η* at low ω and $\dot{\gamma}$ for PA/clay-3 and PA/clay-5. As ω and $\dot{\gamma}$ increase, the deviation between η and η* becomes significant. Interestingly, PA/clay-8 and PA/clay-10 show that the deviation between η and η* is independent of ω and $\dot{\gamma}$. The Similarity failure of the Cox-Merz rule can be observed in nanotube/polypropylene nanocomposites where nanotubes interact with polypropylene

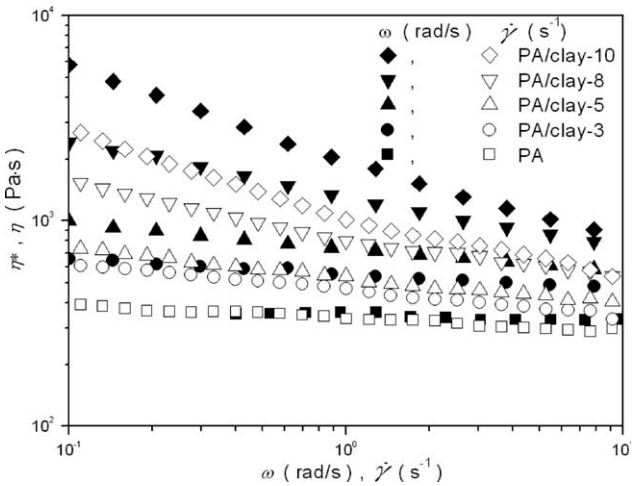

Figure 5 Comparison of dynamic viscosity η* and steady viscosity η of PA/clay under dynamic and steady shear.

and interlock the chains into a microstructure structure.[32] The failure of the Cox-Merz rule can be attributed to the presence of clay interacting with PA. Dynamic shear involves a small deformation under which the microstructure of PA/clay nanocomposites is not completely disturbed. On the other hand, steady shear involves a large deformation, which induced structural changes.

In order to further explore the response of the microstructure, G' and G'' of PA/clay-10 are plotted as a function of the angular frequency for three constant shear rates $\dot{\gamma}$ of 0, 0.01, and 0.1 s^{-1} respectively. Figure 6 shows that G' and G'' of PA/clay-10 significantly decreases at low frequencies with increasing shear rate $\dot{\gamma}$, but all curves converge at high frequencies. G' decreases more rapidly with increasing $\dot{\gamma}$ than G'' at low ω. Generally, the microstructure broken down can be reflected in decreasing G', so a possible reason for the failure of nanocomposites to follow the Cox-Merz rule is that the nanocomposites undergo structure breakdown at large deformation. Thus, dynamic shear may be able to promote the shear thinning capability of the materials. By contrast, steady shear can effectively rearrange molecular packing along the shear direction. Therefore, the resistance to deformation in dynamic shear is greater than that in steady shear. Alternatively, steady shear involves the large strains which induced structural changes. When shear rate and angular frequency are equal, the dynamic viscosity is noticeably larger than the steady viscosity. The modified Cox-Merz rule provides a useful relationship in eq. (8).

$$\eta^* = E\eta^F|_{\omega=\dot{\gamma}} \tag{8}$$

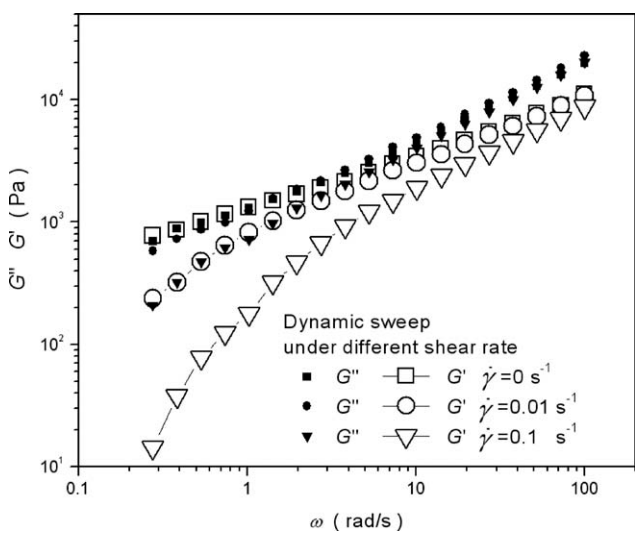

Figure 6 Comparison of elastic modulus G' and viscous modulus G'' of PA/clay-10 in dynamic sweep at different steady shear rate $\dot{\gamma}$.

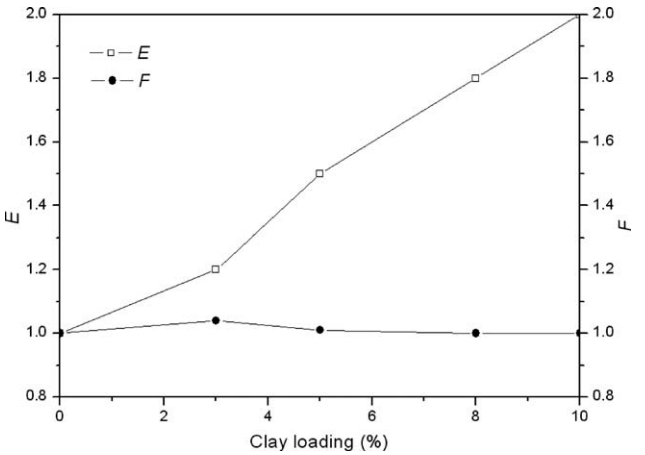

Figure 7 The parameters E and F of the modified Cox-Merz rule.

Power law parameters, E and F, are introduced to provide a more useful correlation. A reasonable approximation of the relationship between η and η^* can be determined by adjusting the power law parameters, E and F. If E and F are set to values of 1, the equation reduces to the Cox-Merz rule. The amount by which these values diverged from 1 indicates that corrections are required for the empirical factors. This equation is widely used for filled systems. The power law index, F and parameter E, can be calculated from eq. (8). The parameters for the modified Cox-Merz rule are shown in Figure 7. The parameter of E increases with clay loading, and F is independent of clay loading. The modified Cox-Merz rule can accurately represent the relationship between η and η^* of PA/clay nanocomposites. The nanocomposites exhibit deviation from the Cox-Merz rule, especially for the sample with high clay loading. This indicates that the addition of clay increases the dynamic viscosity and reflects the thixotropic character of the nanocomposites under large strain deformation. The collapse of network structures and rotation of clay platelets upon steady shear could be a factor for the decrease of viscosity, so clay is responsible for the abnormal deviation between η^* and η at higher clay loading. For dynamic shear, however, such structures maintain their stability and higher complex viscosity is obtained under oscillation deformation.

CONCLUSION

The interaction of PA with clay in nanocomposites is evaluated using a Bohlin Rheometer. The Maron-Pierce model is used to simulate the variation of the effective viscosity (η_r) with volume fraction of clay (Φ_{clay}). The effective volume fraction ($k\Phi_{clay}$) is introduced and the entanglement of PA on clay has to be taken into account. These results and predictions

from the Maron-Pierce model can provide a novel way to build up the relationship of four variables η_r, Φ_{clay}, P, and Φ_c, and evaluate the interaction between PA and clay in nanoscale. The failure of time–temperature superposition (TTS) can be observed in van-Gurp-Palmen plot for PA nanocomposites and the deviations pronounced increases with clay loading. The comparison of dynamic viscosity (η^*) and steady viscosity (η) is carried out according to the Cox-Merz rule. The failure of the Cox-Merz rule can be observed and deviations from the expected behavior increase with clay loading. Therefore, a modified Cox-Merz rule is established. These interesting results indicate that PA/clay nanocomposites are sensitive to shear deformation methods due to the interaction between PA and clay.

References

1. Clifford, M.; Wan, T. Polymer 2010, 51, 535.
2. Krishnamoorti, R.; Vaia, R. A.; Giannelis, E. P. Chem Mater 1996, 8, 1728.
3. Krishnamoorti, R.; Yurekli, K. Curr Opin Colloid Interface Sci 2001, 6, 464.
4. Ren, J. X.; Krishnamoorti, R. Macromolecules 2003, 36, 4443.
5. Galgali, G.; Ramesh, C.; Lele, A. Macromolecules 2001, 34, 852.
6. Giannelis, E. P.; Krishnamoorti, R.; Manias, E. Adv Polym Sci 1999, 138, 108.
7. Zhong, Y.; Wang, S. Q. J Rheol 2003, 47, 483.
8. Krishnamoorti, R.; Giannelis, E. P. Macromolecules 1997, 30, 4097.
9. Krishnamoorti, R.; Ren, J.; Silva, A. S. J Chem Phys 2001, 114, 4968.
10. Pabst, W.; Berthold, C.; Gregorova, E. J Eur Ceram Soc 2006, 26, 1121.
11. Kitano, T.; Kataoka, T.; Shirota, T. Rheol Acta 1981, 20, 207.
12. Marnix, V. G.; Jo, P. Rheol Bull 1998, 67, 5.
13. Doraiswamy, D.; Mujumdar, A. N.; Tsao, I.; Beris, A. N.; Danforth, S. C.; Metzner, A. B. J Rheol 1991, 35, 647.
14. Steffe, J. F. Rheological Methods in Food Process Engineering; Freeman Press: East Lansing MI, USA, 1996; Chapter 5.
15. Dealy, J. M.; Saucier, P. C. Rheology in Plastics Quality Control; Carl Hanser Verlag: Munich, Germany, 2000; Chapter 2.
16. Walter, P.; Trinkle, S.; Suhm, J.; Maeder, D.; Friedrich, C. Macromol Chem Phys 2000, 201, 604.
17. Thomas, D. G. J Colloid Sci 1965, 20, 267.
18. Rutgers, R. Rheol Acta 1962, 2, 202.
19. Rutgers, R. Rheol Acta 1962, 2, 305.
20. Kataoka, T.; Kitano, T.; Sasahara, M.; Nishijima, K. Rheol Acta 1978, 17, 149.
21. Kataoka, T.; Kitano, T.; Oyanagi, Y.; Sasahara, M. Rheol Acta 1979, 18, 635.
22. Kataoka, T.; Kitano, T.; Nishijima, T.; Sakai, T. Rheol Acta 1980, 19, 764.
23. Utracki, L. A. Clay-Containing Polymeric Nanocomposites; Rapra Technology Limited: Shawbury, England, 2004; Chapter 2.
24. Rameshwaram, J. K.; Jeon, H. S.; Weinkauf, D. H. Polymer 2003, 44, 5749.
25. Alexandre, M.; Dubois, P. Mater Sci Eng R Rep 2000, 28, 1.
26. Weon, J. I.; Sue, H. J. Polymer 2005, 46, 6325.
27. Fornes, T. D.; Paul, D. R. Polymer 2003, 44, 4993.
28. Kim, Y.; White, J. L. J Appl Polym Sci 2005, 96, 1888.
29. Van, O. H. An Introduction to Clay Colloid Chemistry: For Clay Technologists, Geologists and Soil Scientists; New York: Wiley, 1977; Chapter 2.
30. Walter, P.; Trinkle, S. Macromol Chem Phys 2000, 201, 604.
31. Doraiswamy, D.; Mujumdar, A. N.; Tsao, I.; Beris, A. N.; Danforth, S. C.; Metzner, A. B. J Rheol 1991, 35, 647.
32. Kharchenko, S. B.; Migler, K. B.; Douglas, J. F.; Obrzut, J.; Grulke, E. A. SPE ANTEC Conf Proc 2004, 2, 1877.